A Four-Port Shared-Aperture In-Band Full-Duplex Antenna Array Based on A Novel Common-Mode and Differential-Mode Combination Method

Yue-Nian Chen, Can Ding, He Zhu, Xiaojing Huang, Yongtao Jia, Ying Liu, and Y. Jay Guo

***Abstract*—In this paper, a four-port shared-aperture in-band full-duplex (IBFD) antenna system is developed based on a novel common-mode (CM) / differential-mode (DM) combination method. By combining the CM and DM of two dual-polarized subarrays, each port of the antenna system excites the entire aperture of the antenna array, leading to the improved gain while maintaining the half-power beamwidth (HPBW) at around 70 degrees. Besides, the intrinsic orthogonality of the two modes leads to low coupling between ports. To verify the proposed method, an IBFD array system, which consists of three modules including differential-fed antenna array, hybrid couplers and power dividers, is designed, fabricated, and measured to realize the shared-aperture excitation from the four ports. Differential feed and decoupling structures are employed to further increase the isolation between ports, which is greater than 38 dB within the bandwidth of 3.3 - 3.8 GHz (14.1%). The gains of all four ports are greater than 8 dBi with more than 20 dB cross-polarization discrimination (XPD). The simulation and experimental results demonstrate great potential of this work in the 5G and beyond sub-6 GHz IBFD systems.**

***Index Terms*—Four-port, dual-polarization, in-band full-duplex (IBFD), common-mode (CM), differential mode (DM), sub-6 GHz.**

I. Introduction

THE increasing number of wireless devices has resulted in a growing problem of spectrum congestion. In-band full-duplex (IBFD), which allows for simultaneous transmission (TX) and reception (RX) of signals in the same frequency, is a promising solution to this issue. However, IBFD is challenging because of the significant self-interference (SI) between TX and RX channels. Self-interference cancellation (SIC) techniques provide an effective solution. The IBFD antenna is the first line of defense against SI, as it can significantly reduce the pressure and complexity of the subsequent SIC techniques in the analog and digital domains [1], [2].

Recently, most existing IBFD antennas have a shared aperture with two ports, one for TX and the other for RX, which can be classified into two categories. As shown in Fig. 1(a), the first type is two-port cross-polarized IBFD antennas, which feature TX and RX ports with orthogonal polarizations [3]–[5]. Additionally, differential feeding can be used to further improve the isolation between polarizations [6]–[9]. The other type is two-port co-polarized IBFD antennas that have both TX and RX ports with the same polarization, as shown in Fig. 1(b). This configuration poses greater challenges due to significant coupling between the two ports with identical polarizations. Additionally, the shared aperture restricts the feasibility of employing decoupling techniques that would normally require additional space. Plenty of effective and interesting methods have been proved effective on this issue, such as isolation feed network consisting of circulators and/or hybrid couplers [10]–[13], antenna modes analysis including eigenmode [14] or characteristic mode [15], [16].

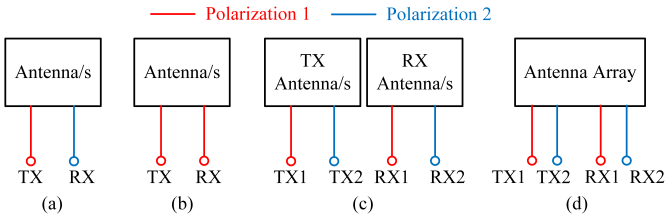

Fig. 1. Schematic diagrams of (a) two-port cross-polarized IBFD system, (b) two-port co-polarized IBFD system, (c) four-port separated-aperture IBFD system, and (d) four-port shared-aperture IBFD system in this work.

However, these two-port IBFD antennas offer only a single polarization for either TX or RX, whereas maximizing spectral efficiency requires polarization diversity. Therefore, a more effective IBFD system should include four channels, each with two orthogonal polarizations for both TX and RX. This configuration is significantly more complex than addressing SI between two ports, as the coupling between different ports involves distinct mechanisms that must be simultaneously addressed using different methods [17]. Although several studies have attempted to address this issue [18]–[21], their performance remains limited. The effectiveness of the SIC techniques in these works heavily depends on the perfect symmetry of the feed network and the balance of component characteristics. Furthermore, while one study successfully realized a four-port shared-aperture IBFD antenna [18], the radiation patterns of the four ports differed, which is undesirable for most applications.

In this paper, it is the first time that a four-port shared-aperture IBFD antenna array with consistent radiation patterns is achieved by employing a novel common-mode (CM)/differential-mode (DM) combination method. Compared to our previous work [21] with a separate aperture design, the shared-aperture antenna system is more challenging, as the spacing between TX and RX antennas is regarded as "0". However, it achieves better performance by improving the aperture utilization efficiency from 50% to 100%. This shared-aperture design enables full aperture excitation in any of the four modes, markedly increasing gain while maintaining the half-power beamwidth (HPBW). Additionally, this work leverages two orthogonal modes to enable high isolation between antenna ports, eliminating the need for complex decoupling structures or networks. This enhances the system's robustness against variations in component performance. The proposed IBFD antenna is designed, fabricated, and measured, and it supports simultaneous transmission and reception in both polarizations from 3.3 to 3.8 GHz (14.1%). The isolation between any two ports is greater than 38 dB.

II. The Proposed CM and DM Combination Method

A. Initial four-port IBFD subarray

Fig. 2(a) depicts a schematic diagram of the initial version of the proposed IBFD antenna system having four isolated ports. The

Manuscript submitted 21 June, 2024. This work was funded in part by the National Natural Science Foundation of China under Grant 62394293 and 62394290, and in part by the 111 Project. (*Corresponding author: Ying Liu.*)

Yue-Nian Chen is with the National Key Laboratory of Radar Detection and Sensing, Xidian University, Xi'an 710071, China, and also with the Global Big Data Technologies Center, University of Technology Sydney, Ultimo, NSW 2007, Australia (e-mail: chenynxxx@126.com).

Can Ding, Xiaojing Huang, and Y. Jay Guo are with the Global Big Data Technologies Center, University of Technology Sydney, Ultimo, NSW 2007, Australia (e-mail: can.ding@uts.edu.au).

He Zhu is with the Manufacturing, Commonwealth Scientific and Industrial Research Organization (CSIRO), Lindfield, NSW 2070, Australia (e-mail:he.zhu@csiro.au).

Yongtao Jia and Ying Liu are with the National Key Laboratory of Radar Detection and Sensing, Xidian University, Xi'an 710071, China (e-mail: liuying@mail.xidian.edu.cn).

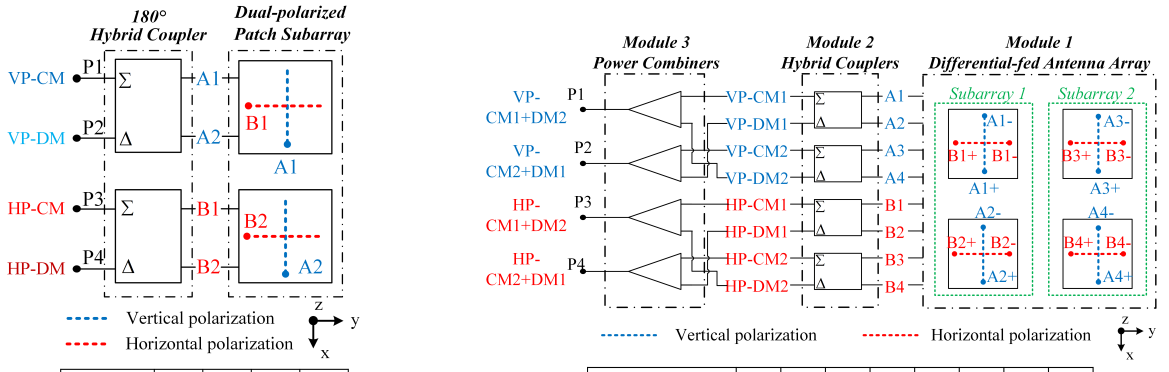

	A1	A2	B1	B2
P1 (VP-CM)	0°	0°	-	-
P2 (VP-DM)	0°	180°	-	-
P3 (HP-CM)	-	-	0°	0°
P4 (HP-DM)	-	-	0°	180°

(a)

	A1	A2	A3	A4	B1	B2	B3	B4
P1 (VP-CM1+DM2)	0°	0°	0°	180°	-	-	-	-
P2 (VP-CM2+DM1)	0°	180°	0°	0°	-	-	-	-
P3 (HP-CM1+DM2)	-	-	-	-	0°	0°	0°	180°
P4 (HP-CM2+DM1)	-	-	-	-	0°	180°	0°	0°

(b)

Fig. 2. Schematic diagrams and output phases of the network of (a) the initial version and the (b) the final version of the four-port IBFD antenna system.

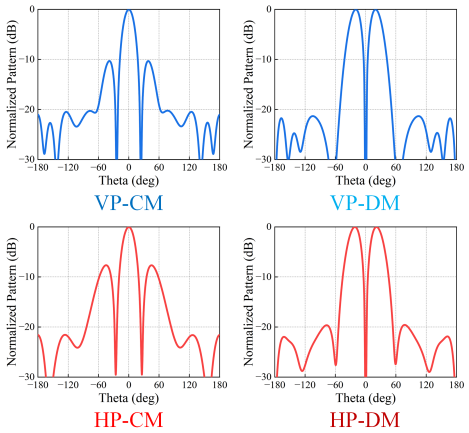

Fig. 3. Radiation patterns of four-port IBFD subarray in the *xoz*-plane.

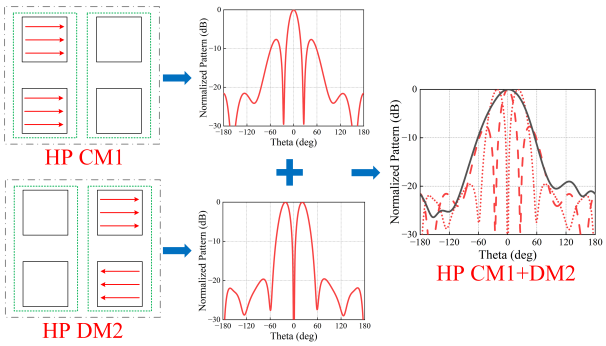

Fig. 4. Current distributions and combined radiation pattern of the proposed IBFD array system when operating in one combined mode.

subarray system comprises two dual-polarized patch antennas and two 180° hybrid couplers to excite the VP and HP, respectively, of the patch array. When exciting the sum (Σ) or differential (Δ) port of a coupler, i.e., P1-P4, the output phases of the network are given in the table, and the patch array is excited in either CM or DM, respectively. In summary, the four ports of the proposed system provide four different operation modes, i.e., *VP-CM*, *VP-DM*, *HP-CM*, and *HP-DM*. The high isolation between the sum and differential ports of the couplers results in a high isolation between the CM and DM modes. Additionally, the VP and HP modes are inherently isolated due to their polarization orthogonality. Therefore, the couplings between the four ports shown in Fig. 2(a) are naturally low in this simple arrangement, which provides a good starting point for the subsequent decoupling efforts.

Despite the preferable high isolation of the subarray, the radiation patterns pose a problem. As shown in Fig. 3, the radiation patterns of the four modes significantly differ from each other, which is undesirable for practical applications. To be specific, the CM modes radiate a boresight radiation beam, while the DM modes produce two split beams. Notably, the spacing between elements is about 1.2 λ, which leads to grating lobes of the array factor at approximately ± 90 degrees in CM. However, the element factor of the patch antenna exhibits low gain at those angles. As a result, the final radiation pattern of the proposed two-element array does not have grating lobes but instead shows side lobes, as shown in Fig. 3. The difference between *VP-CM* and *HP-CM*, as well as *VP-DM* and *HP-DM*, in the radiation patterns arises from the intrinsic disparity between the radiation patterns of the *xoz*-plane and *yoz*-plane for a patch antenna, as shown in Fig. 9(b). Additionally, for VP and HP excitation, the arraying planes differ. Specifically, the VP elements are arrayed along the E-plane, while the HP elements are arrayed along the H-plane.

B. Four-port IBFD antenna system with consistent patterns

To address this issue with the radiation patterns, the CM and DM combination method is proposed, as shown in Fig. 2(b). This system utilizes two subarrays that have been appropriately combined. The main concept is to ensure that any of the four ports excites the two subarrays simultaneously, one in CM mode and the other in DM mode, producing four similar and boresight radiation patterns.

As shown in Fig. 2(b), the IBFD antenna system consists of three modules arranged from right to left. The first module employs two 1×2 patch arrays placed side-by-side. Compared to the patch antennas in the subarray that utilize single feeding, the patch antennas in the array system use differential feeding to enhance the isolation between the two polarizations. In total, there are eight ports (*A1–A4* and *B1–B4*) on the four patch antennas to differentially excite them in two polarizations. The eight ports are connected to the outputs of four 180° hybrid couplers in the second module. The output phases are shown in the table. When any of the eight input ports in the second module are excited, the antenna system operates in eight distinct "singular modes". The third module, which contains four power combiners, combines the eight "singular modes" into four "combined modes" that simultaneously activate both subarrays.

Specifically, when ports 1 – 4 of the array system are activated, the generated "combined modes" are *VP-CM1+DM2*, *VP-CM2+DM1*,

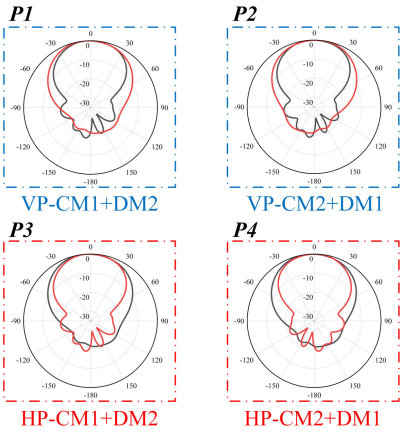

Fig. 5. Radiation patterns of the proposed IBFD array system in the *xoz*- (black lines) and *yoz*- planes (red lines) when operating in the four combined modes.

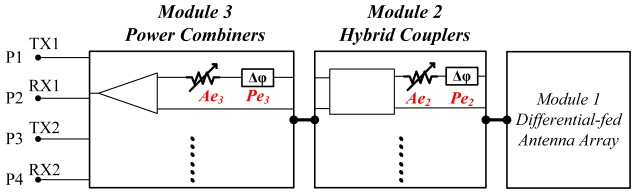

Fig. 6. Adding amplitude and phase errors (*Ae* and *Pe*) to the outputs of the employed components in the three modules.

HP-CM1+DM2, and *HP-CM2+DM1*. Fig. 4 illustrates current distributions and combined radiation pattern of the proposed IBFD array system when operating in *HP-CM1+DM2* as an example. Each "combined mode" activates one vertical subarray in CM and the other in DM, which compensate each other. The corresponding radiation patterns for each mode are shown in Fig. 5. It is worth noting that the radiation patterns in the *yoz*-plane also have similar characteristics due to the geometrical symmetry of the antenna array. The proposed antenna system exhibits CM + DM patterns in both the *xoz*- and *yoz*-planes, which is crucial for maintaining consistent radiation patterns when exciting different ports.

Note that although opposite phase excitation of one patch in our proposed mode combination method will lead to gain loss at the broadside direction, resulting in the deterioration on aperture efficiency compared to the array in uniform phase, this design aims to provide a wide beam for coverage rather than maximizing the gain, which can be particularly important in some applications, such as base stations. Besides, the shared-aperture configuration achieves 100% spatial utilization, whereas the separate-aperture configuration only excites half of the aperture at a time. This is the key advantage of the shared-aperture scheme compared to the separate-aperture scheme.

C. Tolerance to amplitude and phase errors of components

The proposed CM/DM combination method primarily leverages the naturally high isolation between HP and VP, as well as between CM and DM. As depicted in Fig. 2(b), Modules 2 and 3 are directly interconnected, forming the feed network of the shared-aperture array. This feed network's sole purpose is to facilitate the simultaneous excitation of the four orthogonal operational modes, rather than striving for balanced SIC. Consequently, it imposes considerably less stringent demands on component performance. To demonstrate the method's robustness to potential amplitude and phase errors in the employed components, including the hybrid couplers and power combiners, as shown in Fig. 6, we introduced additional amplitude attenuation and phase shifts (*Ae* and *Pe*) at one of the two outputs of these components to assess their effects on the system's isolation performance. It is worth noting that when considering the errors in one module, it is assumed that the errors of each component are the same, and the other modules are error-free for the sake of a clearer comparison. The simulation results, considering these imbalances in Modules 2 and 3, are presented in Figs. 7(a) and 7(b), respectively.

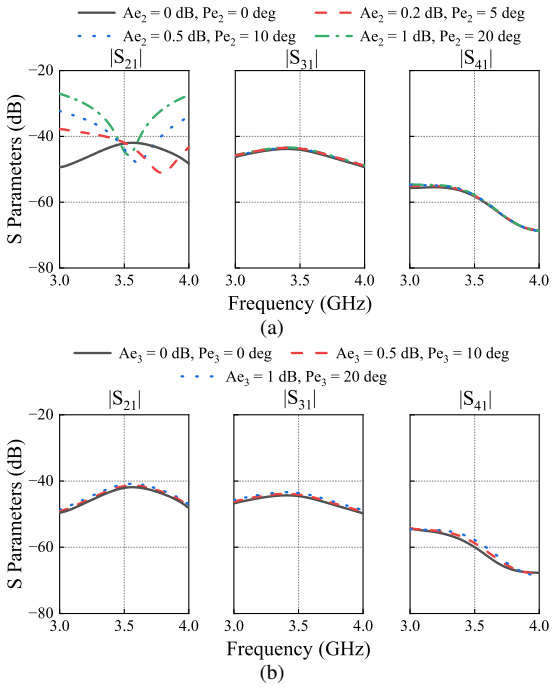

Fig. 7. Simulated transmission coefficients (S_{21}, S_{31}, S_{41}) between the four input ports of the antenna system when amplitude and phase errors exist in (a) Module 2, and (b) Module 3.

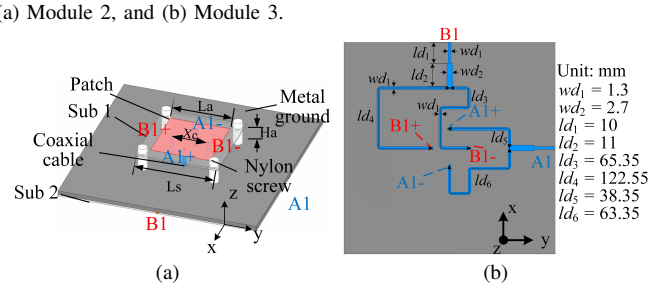

Fig. 8. (a) Perspective view and (b) bottom view of the differential-fed patch antenna element. (Dimensions: *La* = 32 mm, *Ls* = 36 mm, *Xc* = 18 mm, *Ha* = 8 mm)

As depicted in Fig. 7, the isolations between the four IBFD channels remain highly stable, even in the presence of substantial amplitude and phase imbalances. Only potential imbalances in the hybrids in Module 2 can affect S_{21}, which is the coupling between VP ports. It should be noted that S_{43} , which is the coupling between HP ports, has similar performance due to the symmetrical structure. However, the hybrids designed in this work exhibit minimal amplitude and phase errors, thereby minimizing this risk. This system demonstrates much stronger robustness compared to all other cancellation-based IBFD antenna systems, including our previous work [21].

III. Implementation of the IBFD Antenna System

A. Differential-fed antenna element

Figs. 8(a) and 8(b) show the configurations of a single differential-fed antenna element utilized in the IBFD antenna system, which is similar to the one in [21]. The two pairs of feeding ports differentially excite the VP and HP of the patch antenna, respectively. The entire cables pass through the metal ground plane and the outer conductors are connected to the ground plane of differential power divider on Sub 2 that is an Arlon AD440 substrate with a dielectric constant of 4.4 and a height of 0.762 mm. Fig. 8(b) depicts the configuration

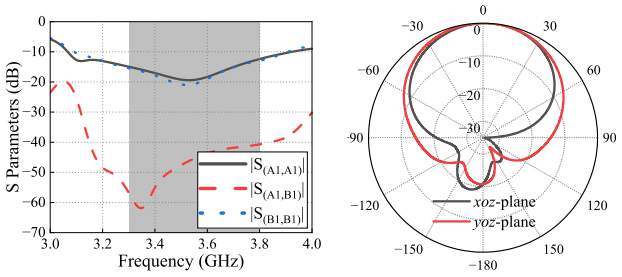

Fig. 9. Simulated results of the patch antenna element. (a) S parameters. (b) Radiation patterns at 3.5 GHz.

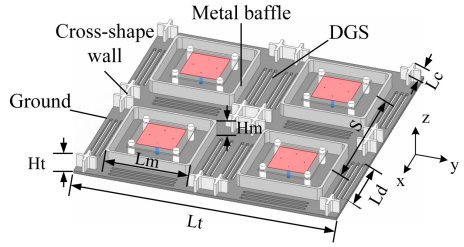

Fig. 10. Configuration of the antenna array with supplementary decoupling structures among patches. (Dimensions: Lt = 200 mm, Lm = 65 mm, Ld = 50 mm, Lc =15 mm, Ht = Hm =10 mm, S = 100 mm)

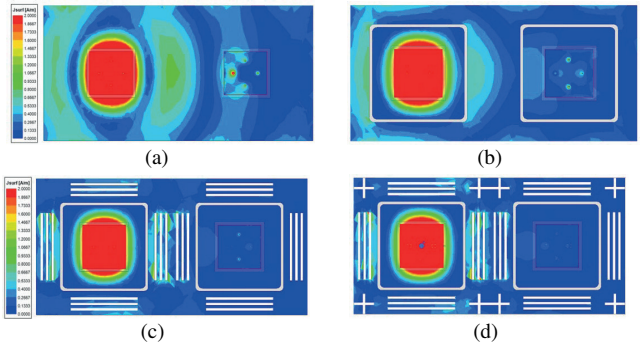

Fig. 11. Current distribution of a subarray at 3.5 GHz when the left patch is excited in HP. (a) *Conf. 1*: without decoupling structures. (b) *Conf. 2*: with metal baffles. (c) *Conf. 3*: with metal baffles and DGSs. (d) *Conf. 4*: with baffles, DGSs, and cross-shaped walls.

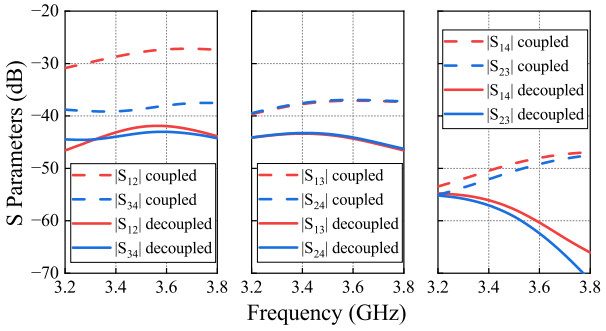

Fig. 12. Comparison of the transmission coefficients between *P1*, *P2*, *P3*, *P4* shown in Fig. 2(b) when the array is coupled and decoupled (without and with the supplementary decoupling structures).

of the differential power divider, which is based on a conventional T-junction power divider [22] with an additional half-wavelength in one branch to introducing a 180° phase difference.

The simulated S parameters of the patch antenna element are presented in Fig. 9(a). It covers an impedance bandwidth of 3.3 – 3.8 GHz for both the HP and VP modes. The isolation between the two polarizations is more than 40 dB within the operation band. Fig. 9(b) depicts the radiation patterns of the VP mode at 3.5 GHz, which exhibit a broadside and symmetrical shape.

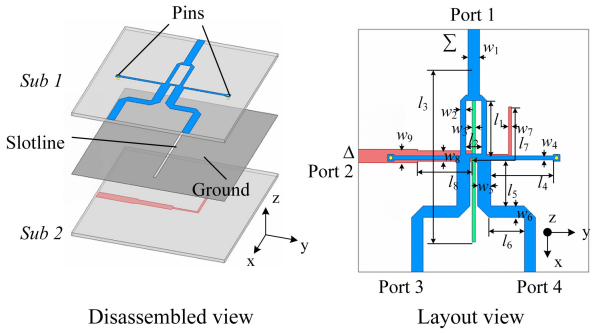

Fig. 13. Configuration of the proposed 180° hybrid coupler. (Dimensions: w_1 = 0.7 mm, w_2 = 0.8 mm, w_3 = 0.5 mm, w_4 = 0.6 mm, w_5 = 2 mm, w_6 = 1.7 mm, w_7 = 0.48 mm, w_8 = 1.56 mm, w_9 = 2.04 mm, l_1 = 8.4 mm, l_2 = 4 mm, l_3 = 26.16 mm, l_4 = 9.5 mm, l_5 = 7 mm, l_6 = 5.4 mm, l_7 = 13.2 mm, l_8 = 8.28 mm)

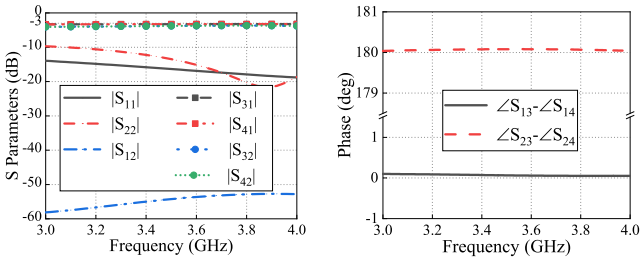

Fig. 14. Simulated results of the proposed coupler. (a) Magnitudes of S parameters. (b) Phase differences between output ports.

B. Antenna array with supplementary decoupling structures

As illustrated in Fig. 10, the antenna array comprises four individual patches and incorporates additional decoupling structures, including metal baffles, defected ground structures (DGSs), and cross-shaped walls, aimed at enhancing isolation among the patches. Note that the distance between elements is larger than one wavelength, which is to enhance the gain of the array while maintaining the HPBW at around 70 degrees. Additionally, this increased spacing is utilized to accommodate additional decoupling structures.

These supplementary structures serve to provide superior shielding for the patch elements, effectively mitigating space waves and surface currents that lead to unwanted couplings. To demonstrate the efficacy of these structures, Fig. 11 showcases the current distribution within a subarray when one patch is excited under various loading conditions. In Fig. 11(a), the absence of these decoupling structures (*Conf. 1*) results in strong induced currents on the right patch when the left element is excited. With the inclusion of metal baffles (*Conf. 2*), Fig. 11(b) indicates significantly reduced current density on the right patch compared to *Conf. 1*. DGSs are introduced at positions with the most significant surface currents in *Conf. 3*. As depicted in Fig. 11(c), the surface currents are effectively trapped within the DGSs, resulting in a significant reduction in coupling between the two patches. *Conf. 4* incorporates cross-shaped walls, which markedly suppress cross-polarized coupling, as shown in Fig. 11(d).

The decoupling achieved between the antenna elements translates into improved isolation between the four ports of the IBFD antenna system shown in Fig. 2(b). Fig. 12 provides a comparison of transmission coefficients between the four ports with and without the inclusion of these decoupling structures. As demonstrated in the figure, these decoupling structures effectively eliminate all couplings, with a particularly significant impact on S_{12}.

C. 180° hybrid coupler

Fig. 13 illustrates the configuration of the designed coupler in the second module, which is similar to the one used in [21]. The

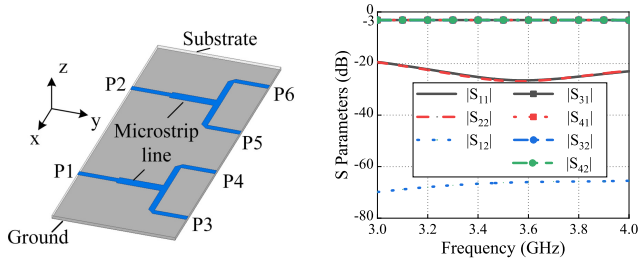

(a) (b)

Fig. 15. (a) Configuration and (b) simulated results of the designed power combiners.

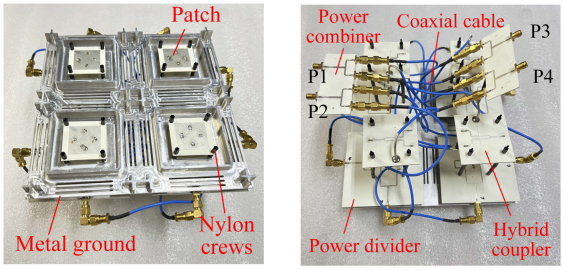

(a) (b)

Fig. 16. Prototype of the fabricated IBFD antenna array system. (a) Top view. (b) Bottom view.

simulated S parameters of the coupler are shown in Fig. 14, covering a wide bandwidth of 3 – 4 GHz with reflection coefficients $<$ -10 dB. The isolation between the sum and differential ports is $>$ 52 dB, and the transmission coefficients from port 1 to the output ports and from port 2 to the output ports are 3.3 dB and 3.8 dB at 3.5 GHz, respectively, remaining stable within the bandwidth. The maximum insertion loss is less than 0.9 dB. As Fig. 14(b) reveals, amplitude and phase imbalances at the two outputs when fed from ports 1 and 2 are within 0.015 dB and 0.1°, respectively.

D. Power combiner

In the third module, four power combiners are required to combine the CM and DM of two subarrays, as shown in Fig. 2(b). The configuration of the designed power combiners is illustrated in Fig. 15(a), where two single traditional T-shape combiners are integrated into one thin substrate with a dielectric constant of 4.4 and a height of 0.762 mm. The simulated results in Fig. 15(b) demonstrate that both power combiners have good impedance matching within the 3 – 4 GHz bandwidth. The insertion loss is consistently below 0.2 dB, and amplitude and phase imbalances are minimal at 0.01 dB and 0.07°, respectively, and the isolation between the two combiners is greater than 65 dB, indicating minimal interference between them.

IV. Experimental Results

As illustrated in Fig. 16, the three modules are fabricated and assembled into a four-port IBFD antenna system. Subsequently, the antenna system undergoes testing in an anechoic chamber.

The simulation and measurement results of the S parameters of the antenna system are plotted in Fig. 17. In general, the measured results agree very well with the simulated ones. The measured bandwidth of all ports can cover the bandwidth of 3.3 - 3.8 GHz. The measured transmission coefficients between the ports with the same polarization (S_{12} and S_{34}) are $<$ -38 dB. Furthermore, the measured transmission coefficients between the ports that excite the orthogonal polarizations (S_{13}, S_{24}, S_{14}, and S_{23}) are $<$ -40 dB. To summarize, the proposed IBFD antenna system provides isolation $>$ 38 dB between any two ports within the desired 5G sub-6 GHz application bandwidth of 3.3 - 3.8 GHz (14% fractional bandwidth).

Fig. 18(a) shows the simulated and measured gains of all ports. The measured gains are more than 8 dBi with the maximum gain

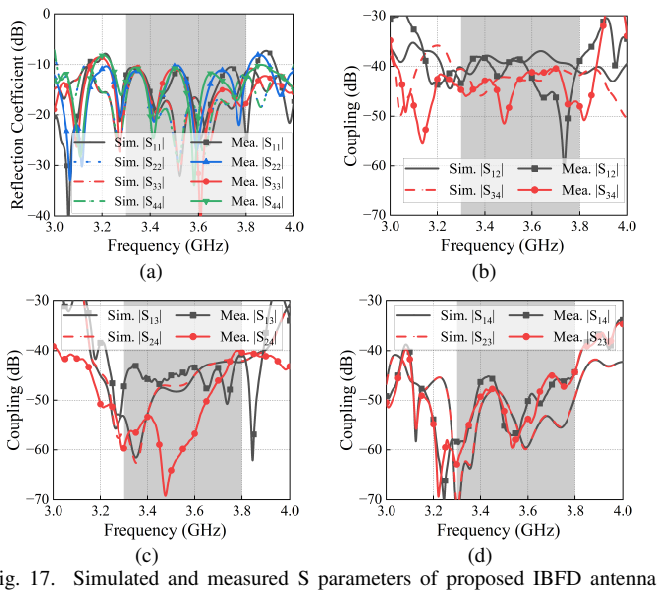

(a) (b) (c) (d)

Fig. 17. Simulated and measured S parameters of proposed IBFD antenna system. (a) Reflection coefficients. (b) Couplings between co-polarized ports. (c) and (d) Couplings between cross-polarized ports.

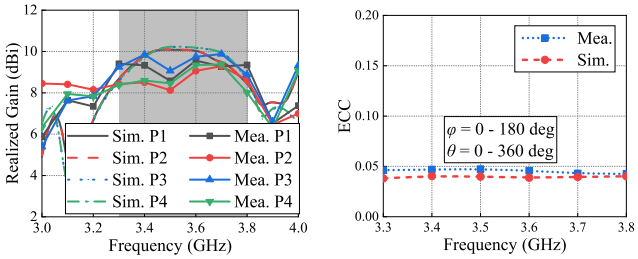

(a) (b)

Fig. 18. Simulated and measured (a) realized gains and (b) ECC between P1 and P2 of the IBFD antenna system.

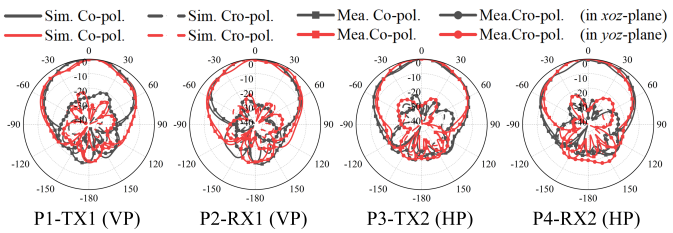

Fig. 19. Simulated and measured radiation patterns of the IBFD antenna system at 3.5 GHz when exciting the four different ports.

of 10 dBi. The measured gains are slightly lower than the simulated ones due to losses introduced by the connection cables. As shown in Fig. 18(b), the envelope correlation coefficient (ECC) between P1 and P2 is $<$ 0.05, which is beneficial for multiple input multiple output (MIMO) system. The low ECC, unlike the result in [18], is due to the excitation of two pairs of orthogonal modes. In Fig. 19, the radiation patterns of all ports at 3.5 GHz are illustrated, where all patterns are broadside and quite similar when exciting different ports. Notably, the HPBWs of all ports are 70 $\pm$ 5 degrees within the operation bandwidth, which is comparable to a single element, ensuring the coverage capability. Besides, due to the employed differential feeding, the cross-polarization discrimination (XPD) is larger than 20 dB for all ports.

There are only a couple of papers that aimed at achieving four channels as this work and a comparison is made in Table I. As demonstrated in the table, the performance achieved by the proposed IBFD antenna system is better than or comparable with that of the state-of-the-art works. Unlike other methods that depend on the

TABLE I
COMPARISON WITH STATE-OF-THE-ART IBFD ANTENNAS WITH FOUR CHANNELS

Ref.	SIC Methods	The Num. of Ant.	Polarizations	Bandwidth	Gain (dBi/dBic)	XPD (dB)	Isolation (dB)	Uniform Radiation Patterns When Exciting Different Ports	Shared Aperture of All Ports
[18]	PO,IFN	1	TX: two CPs RX: two CPs	2 – 8 GHz (120%)	>3	NG	>27	No	Yes
[19]	PO,IFN	TX: 2 RX: 2	TX: two CPs RX: two CPs	6.0 – 6.4 GHz (6.45%)	>7.8	>10	>38	Yes	No
[20]	IFN, NFC	TX: 4 RX: 1	TX: two CPs RX: two CPs	0.8 – 3 GHz (116%)	TX: >4 RX: >-5	>5	>17	No	No
[21]	PO, IFN, DS	TX: 1 RX: 1	TX: ±45° pols RX: ±45° pols	3.3 – 3.9 GHz (16.6%)	>6.2	>18	>39	Yes	No
Proposed	**PO, IFN, DS, CDC**	**TX: 1 RX: 1**	**TX: VP + HP RX: VP + HP**	**3.3 – 3.8 GHz (14.1%)**	$\mathbf{>8}$	$\mathbf{>20}$	$\mathbf{>38}$	**Yes**	**Yes**

PO: polarization orthogonality; IFN: isolation feed network; NFC: near-field cancellation; DS: decoupling structure;
CDC: CM and DM combination; XPD: cross-polarization discrimination = co-pol radiation/cross-pol radiation; NG: not given.

precision of the cancellation network, such as the approach in our previous work [21], this method employs only basic components like power dividers and hybrid couplers, with less stringent performance requirements for these components. Furthermore, this is the first realization of a four-channel IBFD system on a shared-aperture with consistent radiation patterns across all ports. This shared-aperture configuration not only improves the gain—from >6 dBi in the previous separate-aperture design [21] to >8 dBi in this work—but also preserves the HPBW of the radiation pattern. Additionally, the XPD of this work is the largest among these papers, indicating the strong anti-interference capability to the other polarization.

V. CONCLUSION

In this paper, a four-port IBFD antenna array system based on CM and DM combination is proposed, which consists of three modules. The first module is a 2×2 patch antenna array where each element has two pairs of differential ports for VP and HP, respectively. In the second module, four 180° hybrid couplers are used to excite two 1×2 subarrays with CM and DM in VP and HP, respectively. Finally, the power combiners in the third module combine the CM and DM of two subarrays. By connecting all the modules, the designed dual-polarized IBFD system achieves more than 38 dB isolation between any two ports from 3.3 GHz and 3.8 GHz. Furthermore, each port excites the whole array aperture and exhibits similar radiation patterns, making the system a compelling candidate for a wide range of 5G sub-6 GHz applications and is particularly beneficial for base stations due to its coverage capabilities.

REFERENCES

[1] S. Hong, et al., "Applications of self-interference cancellation in 5G and beyond," *IEEE Commun. Mag.*, vol. 52, no. 2, pp. 114–121, Feb. 2014.

[2] Y. Chen, C. Ding, Y. Jia, and Y. Liu, "Antenna/propagation domain self-interference cancellation (SIC) for in-band full-duplex wireless communication systems," *Sensors*, vol. 22, no. 5, pp. 1699, Feb. 2022.

[3] K. -R. Xiang, F. -C. Chen, et al., "Dual-polarized cavity-backed full metal antennas for in-band full-duplex application," *IEEE Trans. Antennas Propag.*, vol. 71, no. 12, pp. 9375-9385, Dec. 2023.

[4] A. Samaiyar, M. Elmansouri and D. S. Filipovic, "Shared-aperture reflectarrays and antenna arrays for in-band full-duplex systems," *IEEE Trans. Antennas Propag.*, vol. 71, no. 11, pp. 9095-9100, Nov. 2023.

[5] K. Y. Yang, W. J. Zhu, L. H. Ye, J. -F. Li and D. -L. Wu, "Metamaterial-based low-profile broadband in-band full-duplex antenna," *IEEE Antennas Wireless Propag. Lett.*, vol. 22, no. 8, pp. 1942-1946, Aug. 2023.

[6] H. Nawaz, N. Ahmad and J. Aslam, "A unidirectional, printed antenna with high interport isolation over wider bandwidth for 2.4 GHz full duplex applications," *IEEE Trans. Antennas Propag.*, vol. 69, no. 11, pp. 7183-7191, Nov. 2021.

[7] M. V. Kuznetcov, S. K. Podilchak, A. J. McDermott, and M. Sellathurai, "Dual-polarized antenna with dual-differential integrated feeding for wideband full-duplex systems," *IEEE Trans. Antennas Propag.*, vol. 69, no. 11, pp. 7192–7201, Nov. 2021.

[8] D. V. S. Prasad, H. V. Singh, S. Tripathi and P. P. Paltani, "In-band full-duplex coradiator antenna with high isolation using differential feed and dual polarization for 2.4 GHz WLAN," *IEEE Antennas Wireless Propag. Lett.*, vol. 22, no. 11, pp. 2740-2744, Nov. 2023.

[9] K. J. Tang, L. H. Ye, W. J. Zhu, J. -F. Li and D. -L. Wu, "Broadband dual-polarized magnetoelectric dipole antenna for in-band full-duplex application," *IEEE Antennas Wireless Propag. Lett.*, vol. 22, no. 9, pp. 2210-2214, Sept. 2023.

[10] P. V. Prasannakumar, M. A. Elmansouri, et al., "Broadband reflector antenna with high isolation feed for full-duplex applications," *IEEE Trans. Antennas Propag.*, vol. 66, no. 5, pp. 2281–2290, May 2018.

[11] P. Valale Prasannakumar, M. A. Elmansouri, L. B. Boskovic, M. Ignatenko, and D. S. Filipovic, "Wideband quasi-monostatic simultaneous transmit and receive reflector antenna," *IEEE Trans. Antennas Propag.*, vol. 68, no. 4, pp. 2630–2637, Apr. 2020.

[12] D. Wu, Y. -X. Sun, R. Lian, et al., "Metasurface antenna with co-circularly polarized radiation characteristics for wideband monostatic simultaneous transmit and receive applications," *IEEE Trans. Antennas Propag.*, vol. 71, no. 4, pp. 3304-3313, April 2023.

[13] W. Kang, J. Mao, Y. Dong and W. Wu, "An in-band co-circularly polarized full-duplex antenna with scattering manipulation," *IEEE Antennas Wireless Propag. Lett.*, vol. 23, no. 1, pp. 79-83, Jan. 2024.

[14] C. J. Ma, S. Y. Zheng and Y. M. Pan, "Millimeter-wave co-polarized in-band full-duplex antenna based on a mode superposition method," *IEEE Trans. Antennas Propag.*, vol. 71, no. 6, pp. 4675-4685, June 2023.

[15] Y. -Z. Liang, F. -C. Chen, et al., "Wideband co-polarized stacked patch antenna for in-band full-duplex applications," *IEEE Trans. Antennas Propag.*, vol. 71, no. 12, pp. 9920-9925, Dec. 2023.

[16] Q. Li and T. -Y. Shih, "Characteristic-mode-based design of planar in-band full-duplex antennas," *IEEE Open J. Antennas Propag*, vol. 1, pp. 329-338, 2020.

[17] Y. -N. Chen, "Differential-Fed Dual-Polarized Antenna Decoupling Techniques for In-Band Full-Duplex," Ph.D. thesis, Univ. of Tech. Sydney, 2024.

[18] E. A. Etellisi, M. A. Elmansouri and D. S. Filipovi´c, "Wideband multimode monostatic spiral antenna STAR subsystem," *IEEE Trans. Antennas Propag.*, vol. 65, no. 4, pp. 1845-1854, Apr. 2017.

[19] M. Ranjbar Nikkhah, J. Wu, H. Luyen and N. Behdad, "A concurrently dual-polarized, simultaneous transmit and receive (STAR) antenna," *IEEE Trans. Antennas Propag.*, vol. 68, no. 8, pp. 5935-5944, Aug. 2020.

[20] M. A. Elmansouri, L. B. Boskovic and D. S. Filipovic, "Compact wideband dual-polarized in-band full-duplex antenna subsystem," *IEEE Trans. Antennas Propag.*, vol. 69, no. 11, pp. 7166-7172, Nov. 2021.

[21] Y. -N. Chen, C. Ding, H. Zhu and Y. Liu, "A ±45°-polarized antenna system with four isolated channels for in-band full-duplex (IBFD)," *IEEE Trans. Antennas Propag.*, vol. 71, no. 4, pp. 3000-3010, Apr. 2023.

[22] S. B. Cohn, "A class of broadband three-port TEM-mode hybrids," *IEEE Trans. Microw. Theory Techn.*, vol. MTT-16, no. 2, pp. 110–116, Feb. 1968.